

Exploitation of Geostationary Earth Radiation Budget data using simulations from a numerical weather prediction model: Methodology and data validation

Richard P. Allan and Anthony Slingo

Environmental Systems Science Centre, University of Reading, Reading, UK

Sean F. Milton and Ian Culverwell

Met Office, Exeter, UK

Received 14 December 2004; revised 17 March 2005; accepted 14 April 2005; published 30 July 2005.

[1] We describe a new methodology for comparing satellite radiation budget data with a numerical weather prediction (NWP) model. This is applied to data from the Geostationary Earth Radiation Budget (GERB) instrument on Meteosat-8. The methodology brings together, in near-real time, GERB broadband shortwave and longwave fluxes with simulations based on analyses produced by the Met Office global NWP model. Results for the period May 2003 to February 2005 illustrate the progressive improvements in the data products as various initial problems were resolved. In most areas the comparisons reveal systematic errors in the model's representation of surface properties and clouds, which are discussed elsewhere. However, for clear-sky regions over the oceans the model simulations are believed to be sufficiently accurate to allow the quality of the GERB fluxes themselves to be assessed and any changes in time of the performance of the instrument to be identified. Using model and radiosonde profiles of temperature and humidity as input to a single-column version of the model's radiation code, we conduct sensitivity experiments which provide estimates of the expected model errors over the ocean of about ± 5 – 10 W m^{-2} in clear-sky outgoing longwave radiation (OLR) and ± 0.01 in clear-sky albedo. For the more recent data the differences between the observed and modeled OLR and albedo are well within these error estimates. The close agreement between the observed and modeled values, particularly for the most recent period, illustrates the value of the methodology. It also contributes to the validation of the GERB products and increases confidence in the quality of the data, prior to their release.

Citation: Allan, R. P., A. Slingo, S. F. Milton, and I. Culverwell (2005), Exploitation of Geostationary Earth Radiation Budget data using simulations from a numerical weather prediction model: Methodology and data validation, *J. Geophys. Res.*, *110*, D14111, doi:10.1029/2004JD005698.

1. Introduction

[2] There are two primary motivations for using Earth Observation data to evaluate the radiation budget in general circulation models. First, radiative processes are crucial in determining the forcing and feedbacks operating on a variety of timescales and therefore make a key contribution both to synoptic-scale evolution and climate change [Intergovernmental Panel on Climate Change, 2001]. Second, the radiative energy emitted and reflected by the Earth-atmosphere system provides a wealth of diagnostic information pertaining to the properties of the atmosphere (e.g., clouds, water vapor and aerosol) and

the surface. High-quality measurements of the Earth's radiative energy budget therefore enable the accuracy of physical processes represented in climate and numerical weather prediction (NWP) models to be scrutinized and improved [e.g., Webb *et al.*, 2001; Haywood *et al.*, 2005].

[3] Measurements of the Earth's top of atmosphere (TOA) radiation budget from satellites in low Earth orbit (LEO) are commonly used to test the realism of clouds, water vapor and the energy budget in climate models [e.g., Kiehl *et al.*, 1994; Pope *et al.*, 2000; Soden *et al.*, 2002]. Such analyses are often confined to long-term means (e.g., monthly to decadal) and over coarse grids, in part because of the limitations of time and space sampling imposed by the orbit [e.g., Wielicki *et al.*, 1996]. This can lead to problems in understanding the reasons for differences

between models and data due to the disparate sampling [e.g., *Allan and Ringer, 2003*] and also because the radiative interactions that determine how physical processes operate occur on much shorter timescales (e.g., hours to days) than those usually considered. To avoid some of these limitations, one approach is to exploit the data from geostationary satellites which, over the portion of the earth visible from the satellite, do not suffer from the spatiotemporal sampling problems of LEO satellites.

[4] While both geostationary and LEO satellite data are utilized extensively through data assimilation to provide the initial conditions for NWP models, less use has been made of the data in evaluating these models. However, the potential for this application is considerable, since data that have not been used to initialize the forecast have a valuable role to play in verification. This is particularly important for clouds, information on which can readily be retrieved from satellite imagery, although methods for including this information in the data assimilation process are still under development. Satellites can therefore provide an independent source of data for evaluating the representation of clouds in NWP models. The nature of such an evaluation can be quite distinct from that employed when testing a climate model; in NWP, it is possible to perform a series of instantaneous comparisons for specific times and thereby to examine the high-frequency behavior of the model, as opposed to the time-averaged comparisons typically performed with climate models. Nevertheless, the similarity between the physical parameterizations now employed in the two classes of model ensures that lessons learnt with one version are relevant to the other. There are some potential caveats to this argument. For example, there is evidence to show a dependence of moist processes, including cloud cover, on model vertical resolution [*Bushell and Martin, 1999; Lane et al., 2000*] and spatial resolution [e.g., *Kiehl and Williamson, 1991; Phillips et al., 1995*]. However, recent studies by *Pope and Stratton [2002]* with the Met Office climate model show relatively small changes in cloud fraction with spatial resolution. Also, the Met Office climate and global NWP versions are currently run with the same 38 vertical levels.

[5] Motivated by the above reasoning, we have initiated a project to compare simulations from the Met Office NWP model with data from the new Meteosat-8 geostationary meteorological satellite [*Schmetz et al., 2002*]. Comparisons are undertaken on a near real-time basis (e.g., within one day), which allows timely feedback on the quality of both the satellite data and the model simulations in relation to the current synoptic situation. The project has the acronym SINERGEE (Simulations from an NWP Model to Exploit Radiation Data from a New Geostationary Satellite, Explore Radiative Processes and Evaluate Models). The acronym reflects the intention to enhance the synergy between the models used for numerical weather and climate prediction and Earth Observation satellite data. Potential applications include observational studies of the physical processes important for accurate simulations of weather and climate, evaluation of the performance of the NWP model and the potential for contributing to the calibration and validation of the satellite instruments.

[6] In this paper we describe the methodology and first comparisons between simulations from the Met Office NWP model and broad-band radiation budget data from the Geostationary Earth Radiation Budget (GERB) instrument on Meteosat-8 [*Harries et al., 2005*]. This is the first such instrument to be flown in geostationary orbit, providing unprecedented temporal sampling of the radiation budget. As a particular focus of the present study, we concentrate on comparisons of clear-sky radiative fluxes over the ocean. These model fields are likely to be well constrained by the surface and atmospheric properties due in part to the data assimilation employed. Additionally, objective estimates of model error may be computed for example using the observed and analyses profiles of temperature and humidity. Therefore such comparisons provide an important consistency check for the radiative fluxes derived from the GERB instrument. The following section describes the NWP model and the GERB data used in the comparisons. The methodology is discussed in section 3 and initial results are presented in section 4. Comparisons of clear-sky fluxes over the ocean are conducted in section 5. A general discussion of the results of this study and plans for future work are presented in section 6.

2. Model and Data

2.1. Met Office Forecast Model

[7] The version of the Met Office operational global NWP model used here was introduced in August 2002 (cycle G27). The horizontal resolution is 0.833 degrees in longitude and 0.556 degrees in latitude, equivalent to about 60 km at midlatitudes. There are 38 vertical levels with a top at 3 hPa. The model is based around a new dynamical core which is nonhydrostatic and uses a two time level, semi-implicit, semi-Lagrangian formulation. The basic time step is 20 minutes. In the vertical, a Charney-Phillips grid staggering is used (potential temperature and vertical velocity are on the same half levels, whereas pressure, wind components, etc are on the full model levels). The vertical coordinate is height, but a hybrid approach provides the usual terrain-following grid near the surface. In the horizontal, the Arakawa C grid staggering is used. Further details of the model and the background for this approach are discussed by *Bell et al. [2002]*.

[8] The starting point for the physical parameterizations in the NWP model was version HadAM3 of the climate model [*Pope et al., 2000*], updated to include the revisions in version HadAM4 [*Webb et al., 2001*]. The radiation code is described by *Edwards and Slingo [1996]*, the mixed phase cloud and precipitation scheme is described by *Wilson and Ballard [1999]*, and the nonlocal boundary layer scheme is described by *Lock et al. [2000]* and *Martin et al. [2000]*. Further modifications have been made to improve the triggering, closure, and definition of convection. A separate diagnosis for shallow convection is introduced with cloud base closure according to *Grant [2001]* and entrainment rates from *Grant and Brown [1999]*. The CAPE closure of *Fritsch and Chappell [1980]* is used for deep convection. The orographic gravity wave drag scheme is described by *Webster et al. [2003]*, and that for orographic roughness is described by *Milton and Wilson [1996]*. The land surface scheme is MOSES II

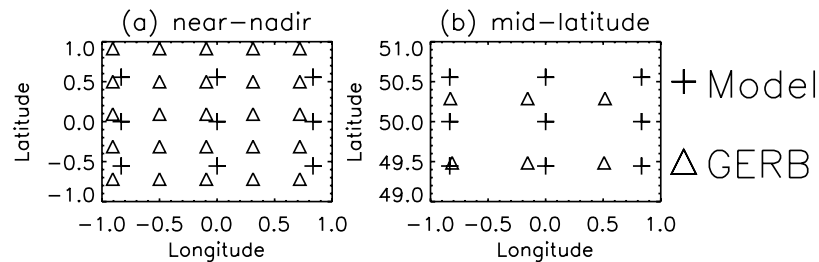


Figure 1. Comparison of model and GERB (BARG) grids for (a) near-nadir and (b) midlatitude regions.

(Met Office Surface Exchange Scheme, version 2), which allows for surface heterogeneity effects within a grid box through a tiling approach [Essery *et al.*, 2003]. The three-dimensional variational data assimilation scheme is described by Lorenc *et al.* [2000].

2.2. Geostationary Earth Radiation Budget (GERB) Experiment

[9] The GERB instrument was launched on board Meteosat-8 in August 2002. Using a 256-element detector array, GERB measures the total and shortwave broadband radiances emitted and reflected from the Earth; longwave radiances are calculated by subtraction of the shortwave from the total. The measurements are internally calibrated on the satellite using a black body source and an integrating sphere illuminated by the sun. The radiances are converted to radiative fluxes at the top of the atmosphere using angular models which depend on the scene type, identified by the high resolution imager on Meteosat-8 [Ipe *et al.*, 2004]. This aspect of the data processing is performed at the Royal Meteorological Institute of Belgium (RMIB).

[10] In the present study, we use the Level 2 averaged, rectified, geolocated product (ARG), which is based on 6 scans at an approximate time resolution of 17 min and a nominal spatial resolution of 50 km at the subsatellite point. Additionally, we also use Level 2 BARG data, which are available in exact 15 minute time bins with an exact subsatellite spatial resolution of 50 km. These data are preliminary; full data release is expected in 2005 following

successful and necessary validation. Further details of the instrument, processing system, data products, and initial validation are given by Harries *et al.* [2005].

3. Methodology

[11] The NWP model is initialized using 3 dimensional variational assimilation to produce analyses four times each day, from which forecasts are integrated. These operational forecasts are produced to a stringent schedule which does not allow the provision of expensive additional diagnostics, since these could delay the forecast process. A solution employed here and in other diagnostic projects at the Met Office is to run additional single time step integrations independently of the main forecast model run, using the operational analyses as initial conditions. Extra diagnostics may thus be obtained without interfering with the forecast process.

[12] In the present study we analyze only the output from the first time step following initialization. A limitation of this methodology relates to model spin-up: are the moist processes from a one time step run from model analysis representative of model errors at later forecast ranges or are they dominated by physical-dynamical imbalances in the initial state? The global NWP model does suffer from a spin-up with cloud cover increasing in the first 24 hours of the forecasts. However, the pattern of spatial and temporal errors (model minus GERB) are not greatly altered by this spin-up which tends to be an uplift in cloud cover across the

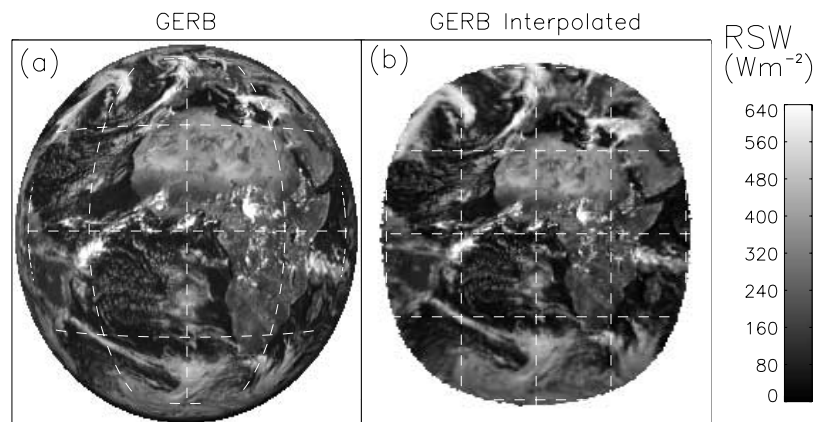


Figure 2. Reflected shortwave radiative flux (RSW) from GERB for (a) the BARG grid and (b) interpolated to the model grid for 1200 UTC, 21 April 2004. Dashed lines represent lines of equal longitude and latitude spaced by 30°. See color version of this figure in the HTML.

Table 1. GERB Level 2 Radiative Flux Product Summary

Dates	Version	Notes
23 May 2003 to 14 Aug 2003	1-MS7A	Meteosat-8 at 10.5°W, Meteosat-7 processing
15 Aug 2003 to 6 Nov 2003	—	no data: sunblock mode
7 Nov 2003 to 31 Dec 2003	2-MS7A or 2-SEV1	improved geolocation, SEVIRI processing begins
23 Dec 2003	2-SEV1	improved time interpolation
Jan 2004	2-SEV1	Meteosat-8 moves from 10.5°W to 3.4°W
20 Jan 2004	2-SEV1	improved geolocation
9 Mar 2004	2-SEV1	SEVIRI cloud mask correction
Apr 2004	2-SEV1	no 0000 UTC data: Sun avoidance
22 Apr 2004	2-SEV1	improved geolocation
26 May 2004	—	model update: assimilation of new satellite data (AIRS)
1 Aug 2004 to 21 Sep 2004	—	no data: sunblock mode
29 Sep 2004	2-SEV1	thin cirrus correction, BARG angular correction
5 Oct 2004	—	model update: 4-D variational data assimilation introduced
11 Oct 2004	2-SEV1	correction: Sun glint
22 Sep 2004 to 31 Oct 2004	2-SEV1	no 0000 UTC data: Sun avoidance
20 Dec 2004	2-SEV1	shortwave flux modification
18 Jan 2005	—	model update: microphysics and boundary layer scheme; increase in surface albedo over Sahara
9 Feb 2004 to 1 Mar 2005	2-SEV1	no 0000 UTC data: Sun avoidance

whole field. This issue will be further addressed in future work to look at cloud and radiation in the forecasts.

[13] At ESSC, the model diagnostics are acquired automatically from the Met Office. In parallel, data from GERB corresponding to the time of the model data are transferred automatically from RMIB. The most recent GERB data available are ingested and interpolated onto the model grid. Figure 1 compares the model and GERB (BARG) grids for a near-nadir region and a midlatitude location. While the GERB resolution is higher than the model resolution for near-nadir locations, the resolution at higher latitudes is comparable between model and data. Figure 2 illustrates the interpolation of the data from the GERB grid (Figure 2a) to the model grid (Figure 2b) for the reflected shortwave radiation (RSW) field.

[14] The timing of the model and satellite data is similar but not identical. The model data range from the analysis time (e.g., 1200 UTC) to 20 min afterward, while the satellite data may be valid for 1200–1215 UTC, for example. The outgoing longwave radiation (OLR) from the model is an average of the beginning and end of the 20 minute time step. The homogeneity of the longwave radiation fields means that the differences due to the disparate timing between the model and the data are small. However, with regard to shortwave comparisons, the timings are crucial due to the large changes in solar zenith angle over the course of the day. In the model, shortwave fluxes are calculated using an average solar zenith angle for the time step, while for the GERB data the precise timing depends on the product.

[15] It is also instructive to represent the RSW as a fraction of the incoming solar radiative flux at the top of the atmosphere (ISW). The ISW valid for the data time range of each GERB pixel is calculated as,

$$ISW(\psi, \phi, t) = S\epsilon(t)\mu(\psi, \phi, t), \quad (1)$$

where S is the solar insolation at the mean Earth-Sun distance and is set to 1365 W m^{-2} for consistency with the model. ϵ is the orbital scaling factor which takes account of the varying Earth-Sun distance and includes the equation of time, and μ is the cosine of the solar zenith angle which is a

function of the sine of the solar declination, longitude (ψ), latitude (ϕ) and time (t). From this, the albedo (α) may be computed as,

$$\alpha(\psi, \phi, t) = RSW(\psi, \phi, t)/ISW(\psi, \phi, t). \quad (2)$$

[16] The model and GERB outgoing longwave radiation and albedo fields are then compared and the images stored. The colocated model and satellite gridded data are also stored for future use. Level 2 ARG and BARG data are included in the processing. Because ARG data times are not fixed for exact 15 minute bins, it is necessary to calculate corresponding ISW fluxes separately for each of the 256 detectors using equations (1) and (2).

3.1. Preliminary Data Issues

[17] In the present study we examine preliminary versions of the GERB data, provided by RMIB. Table 1 summarizes these data versions and details of the Meteosat-8 satellite position and missing data periods. Variation in the quality of these versions of the GERB data are likely to relate to geolocation errors, artifacts for example caused by mis-registration of the imager data employed, changes of geometry between the GERB instrument and the imager on Meteosat-8 and the imager on board Meteosat-7 at 0° , 0° . Additional errors due to stray light infiltrating the detector or spectral response uncertainty will also affect the accuracy of the GERB level 2 fluxes.

[18] The processing system for GERB is designed to use data from the Spinning Enhanced Visible and Infrared Imager (SEVIRI), the primary operational meteorological instrument on Meteosat-8, in the radiance to flux conversion process (SEV1 [Ipe et al., 2004]). However, for much of 2003 there was limited availability of the SEVIRI data as the instrument had not yet become operational. Imager data from the Meteosat-7 satellite (MS7A) were therefore used. The version 1-MS7A data contain an angular mismatch between the GERB instrument at 10.5°W and the Meteosat-7 imager used at 0°W , have large geolocation errors and numerous data artifacts. Version 2-MS7A or SEV1 products contain an improved geolocation algorithm and far less missing data. Further improvements to geolocation, temporal interpolation

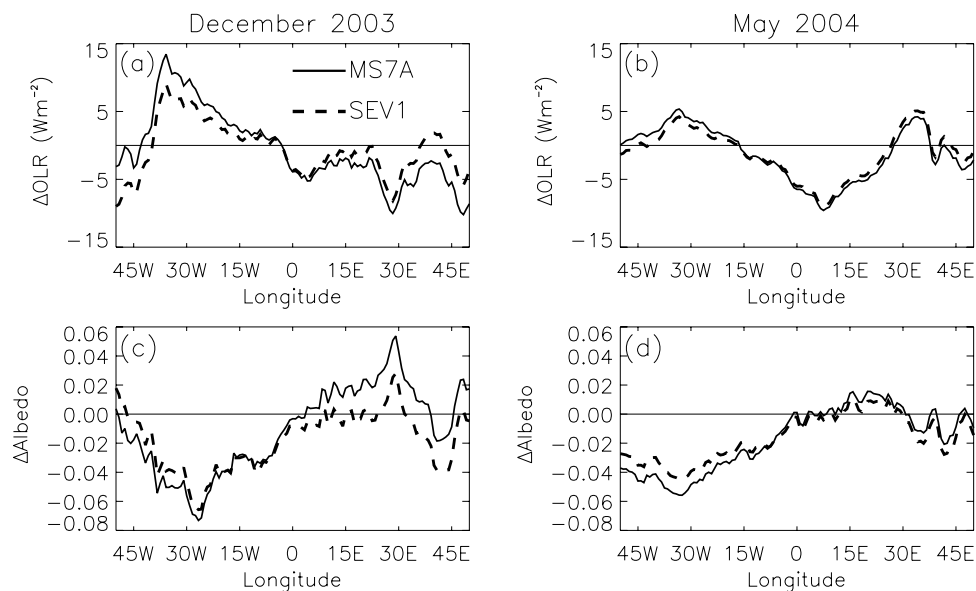


Figure 3. GERB minus model (a and b) OLR and (c and d) albedo differences using MS7A and SEV1 processing of GERB BARG data for (left) December 2003 and (right) May 2004. Only grid points with viewing zenith angles less than 75° are considered.

and radiance to flux conversion accuracy were applied by RMIB to the version 2-SEV1 data throughout the 2003–2004 period (Table 1).

[19] Figure 3 shows the impact of the radiance to flux conversion on the meridional mean GERB (BARG) minus model OLR and albedo differences for December 2003 and May 2004, for both MS7A and SEV1 processed data. The model effectively provides a benchmark from which to compare the two flux estimates. Analysis of the GERB fluxes in December 2003 and May 2004 using either Meteosat-7 (version 2-MS7A) or SEVIRI (version 2-SEV1) imager data for processing suggest that differences are small within about 15° of the Greenwich meridian. Further west than 15°W , longwave fluxes using MS7A processing are overestimated by about 5 W m^{-2} and further east than 15°E version 2-MS7A longwave fluxes are underestimated by about 5 W m^{-2} compared to those using SEVIRI imager processing for December 2003 (Figure 3a). For May 2004 (Figure 3b) these differences are of the same sign but of smaller magnitude (about 1 W m^{-2}). This may reflect the angular differences between GERB/SEVIRI and the imager on Meteosat-7 which are 10.5° apart in December 2003 but only 3.4° different in May 2004. For December 2003, GERB albedo estimates using MS7A processing are about 0.01 lower further west than 15°W and about 0.02 higher further east than 10°E compared to the SEV1 processed data (Figure 3c). Again, the albedo differences for May 2004 are similar but of smaller magnitude (Figure 3d). Albedo estimates over eastern Europe appear to be overestimated by 0.1 using MS7A processing compared with SEVIRI processing for December 2003 (not shown) and the albedo differences are larger when considering high solar zenith angles.

[20] Although model errors in radiative fluxes are likely to be large, particularly where errors in model cloud or aerosol are large [e.g., Haywood *et al.*, 2005], it is note-

worthy that the GERB minus model OLR and albedo differences are smaller when using the SEVIRI radiance to flux processing compared to the MS7A processing. The GERB minus model differences are also generally smaller for May 2004 compared to December 2004, which may reflect the improved quality of the more recent data when Meteosat-8 had achieved its nominal position of 3.4°W . Therefore, in the present assessment of the preliminary data it is important to consider their quality as a function of both time and of viewing angle.

4. Initial Comparisons of GERB and Model Radiation Budget

[21] We now present seasonal mean and instantaneous comparisons between the preliminary GERB data and the model simulations using version 2-SEV1 BARG GERB data.

4.1. Instantaneous Comparison

[22] Figure 4 shows OLR and albedo for GERB BARG data (Figure 4, left) and model (Figure 4, right) for 1200 UTC on 31 March 2004. Although global data are provided by the model, the GERB missing data mask is applied to aid the comparison. For the OLR comparison (Figures 4a and 4b) lower values correspond primarily with the coldest, high-altitude cloud tops. The highest values originate over clear-sky regions of Africa, where the low atmospheric transmission allows emission from lower, warmer layers of the atmosphere. This is enhanced by the high surface temperatures over the clear-sky land at 1200–1220 UTC, due to strong solar heating of the surface. The lowest OLR tends to correspond with the brightest albedo in Figures 4c and 4d. This is due to optically thick cloud associated with deep tropical convection and large-scale midlatitude weather systems. However, regions of low-

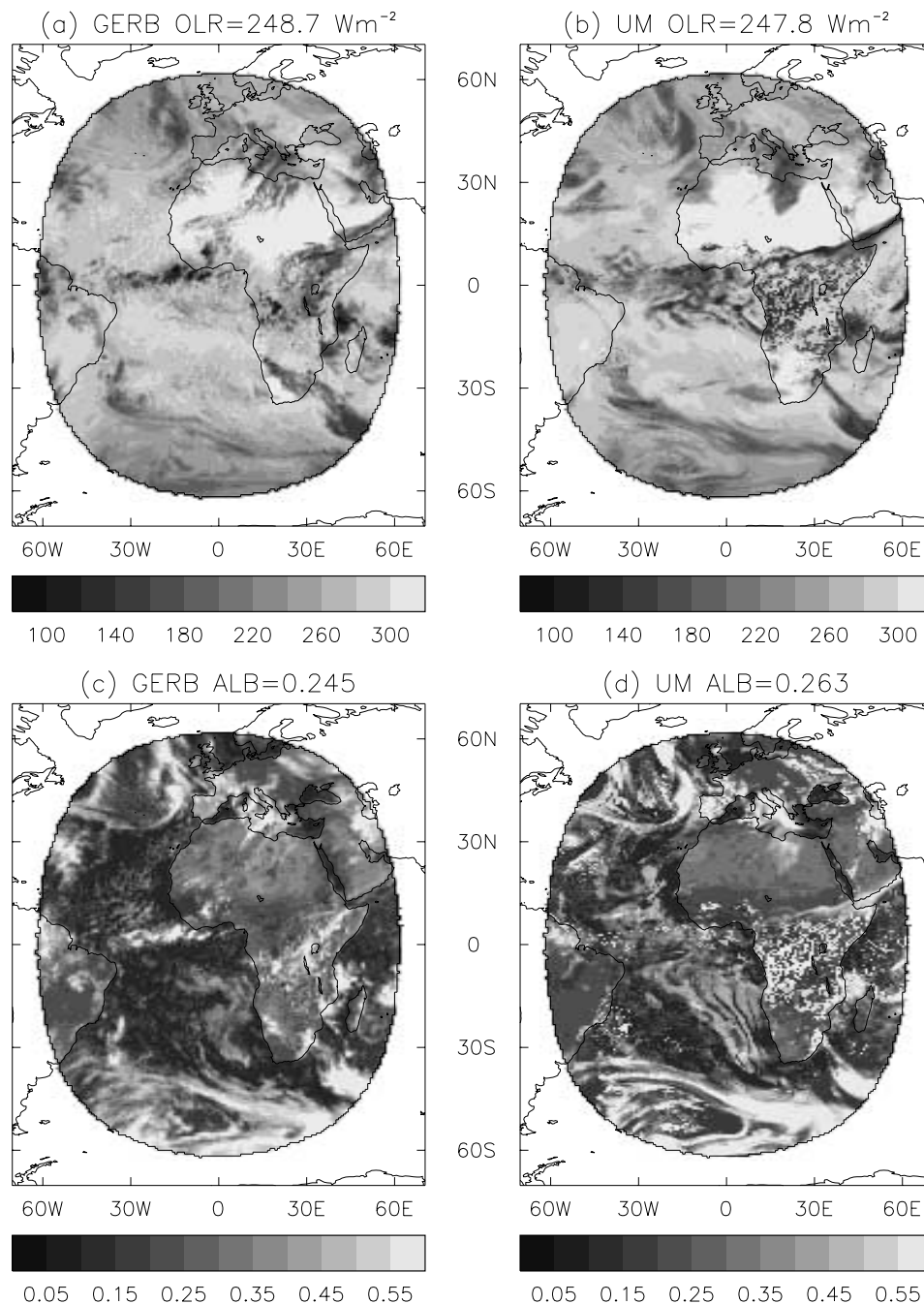


Figure 4. Example comparison of observed (BARG) and simulated OLR and albedo fields over the region viewed by GERB for 31 March 2004 at 1200 UTC. See color version of this figure in the HTML.

altitude cloud (e.g., stratocumulus at 0°W , 15°S) and desert surfaces (e.g., the Sahara) are also highly reflective, as well as contributing to high OLR.

[23] In general, the comparisons in Figure 4 show excellent agreement between the model and GERB data. In particular, for the middle and high latitudes the top of atmosphere radiative energy fluxes appear to be well simulated by the model. This indicates that the simulation of the large-scale atmospheric dynamics is well constrained by the model's assimilation system, resulting in a reasonable distribution of atmospheric humidity. The model's cloud

parameterizations are then able to convert this information into realistic cloud fields.

[24] Over lower latitudes, however, the simulation of OLR and albedo by the model are less satisfactory. For example, over equatorial Africa, the model OLR is underestimated and the albedo overestimated at this time. This relates to an inaccurate representation of the diurnal cycle of convection, a common feature in both NWP and climate models [e.g., *Slingo et al., 2004; Morcrette, 1991; Yang and Slingo, 2001*]. The observed distribution of convective cloud also appears to be more organized spatially than in

the simulations. Further differences between the model and the data include the distribution of marine stratocumulus cloud over the south Atlantic and of convective cloud over the intertropical convergence zone (ITCZ), differences in the albedo and OLR over the Sahara, and an underestimate of convection over Brazil [see also *Allan et al.*, 2004b].

4.2. Seasonal Mean Comparison

[25] Although it is important to consider high time resolution variability, by analyzing model observation differences over longer timescales systematic differences may be identified. These may then be attributed to model or observation errors by considering higher time resolution data. Figure 5 shows the GERB (BARG) and model OLR and albedo for December 2003 to February 2004 (DJF). Averages are constructed separately for each analysis time (0000, 0600, 1200, and 1800 UTC) and then combined to produce the mean OLR, RSW and ISW. Albedo is then calculated using equation (2). Also shown are DJF 2003/4 means from the CERES instrument on the Aqua satellite (CERES/AQUA ERBE-like version 2 ES4 FM-3 data). The CERES ERBE-like data use extensive diurnal modeling to construct monthly daily means which is likely to introduce errors. However, comparison of the overall seasonal mean distribution of radiative fluxes provides an important consistency check on both the GERB and CERES data. To aid comparison, all data are presented on the 2.5° latitude by 2.5° longitude CERES grid using the GERB missing data mask.

[26] Consistent with the instantaneous comparisons between model and GERB data in Figure 4, the model simulated albedo over the Sahara is lower than the GERB and CERES observations and the model appears to overestimate the albedo over the Atlantic marine stratocumulus regions (Figures 5b and 5d). The GERB albedo values are also systematically larger than the model values at sunset and, in particular, at sunrise.

[27] The CERES and GERB observed distribution of OLR over tropical Africa is not well represented by the model simulations. The observed minimum in OLR, corresponding with a convectively active regime, is of smaller magnitude in the model (Figure 5a) suggesting that deep convective cloud is underestimated by the model when averaging over a month for all analysis times. The reverse situation is apparent in Figure 4 for the instantaneous comparison at 1200 UTC, with the model overestimating albedo and deep convective cloud while underestimating OLR. Analyzing the remaining analysis times (0000, 0600 and 1800 UTC) shows an overestimation in OLR and underestimation in albedo over tropical Africa by the model (not shown). Thus the monthly mean comparison shown in Figure 5 include model biases due to errors in the timing of convection causing an underestimation in OLR at 1200 UTC and a residual overestimation in OLR denoting underactive convection in the model at other times. The nature of these errors may alter (spin-up) as the forecast progresses; this is beyond the scope of the present study.

[28] Across eastern Europe and also toward the western limb (50°W), GERB OLR appears lower than the model and CERES suggesting there may be issues relating to the accuracy of GERB fluxes for higher viewing angles.

Nevertheless, it is important to note that, despite the inconsistent spatiotemporal sampling for the CERES instrument, there is generally good agreement between the DJF OLR and albedo fields (Figures 5c–5f), showing that neither CERES nor GERB data are grossly in error. More detailed comparisons of the GERB and CERES data are currently being undertaken elsewhere [e.g., *Harries et al.*, 2005].

4.3. Model Evaluation

[29] While the potential for using comparisons such as those presented in Figures 4 and 5 in model evaluation is considerable [*Allan et al.*, 2004b], this is beyond the scope of the present study. More extensive examination of the model limitations will be detailed elsewhere following successful validation of the GERB data. For the remainder of the present paper, we focus on the validation of clear-sky fluxes over the ocean derived from GERB using model simulations of clear-sky radiation fields and additional statistical information, generated during the forecast model verification process, including vertical profiles of temperature and humidity from radiosonde soundings.

5. Validation of Clear-Sky Fluxes Over the Ocean

[30] The previous section illustrates that the representation of clouds still presents a major challenge to numerical weather prediction. In part, this is because the existence of clouds within a model grid box must be parameterized from the resolved-scale model fields and there is no established theory for how to do this. In contrast, clear-sky simulations over the oceans should be much more accurate, for three main reasons. First, data assimilation methods are extremely successful in minimizing errors in the temperature and humidity fields in model analyses, as is shown below. Second, over the oceans, surface temperatures are analyzed and the albedo of the ocean surface well understood. Third, the radiation codes currently used in NWP and climate models can reproduce the results from much more detailed reference codes with high accuracy [*Edwards and Slingo*, 1996]. Clear-sky radiation budget simulations over the oceans are therefore likely to be much more accurate than for cloudy conditions and should thus facilitate independent validation of the quality of the GERB data and of any changes in time. This conclusion is supported by the analysis of clear-sky fluxes in the ECMWF 40-year reanalysis project, reported by *Allan et al.* [2004a]. It was therefore decided to utilize the clear-sky fluxes generated by the forecast model, along with statistical information on the accuracy of model temperature and moisture profiles, as a way of assessing the quality of clear-sky fluxes produced from the GERB data.

5.1. Estimates of Model Flux Error

[31] To estimate the likely error in model clear-sky fluxes over the ocean, we consider a number of island or coastal locations where information is available from the data assimilation data sets on the model error in temperature and moisture vertical profiles. These stations and their locations are listed in Table 2. We use model verification statistics and additional considerations of likely model errors to perform a range of sensitivity tests for one month

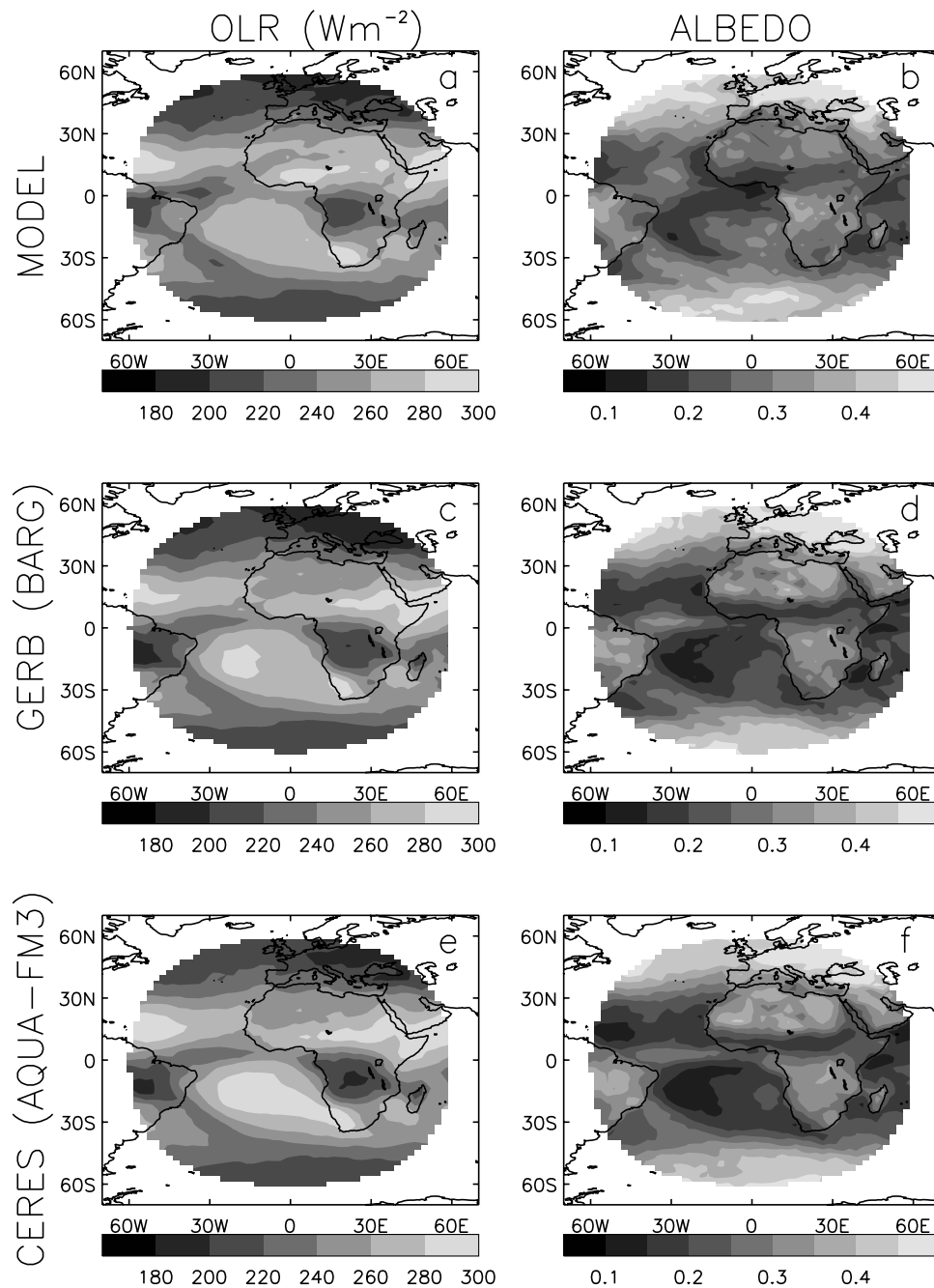


Figure 5. December 2003 to February 2004 mean OLR and albedo for (a and b) model, (c and d) GERB (BARG), and (e and f) CERES on Aqua. The Model and GERB data are constructed from the four model analysis times (0000, 0600, 1200, and 1800 UTC) and interpolated to the CERES 2.5° by 2.5° grid. See color version of this figure in the HTML.

of data, thereby allowing an estimation of the likely errors in simulated clear-sky fluxes over the ocean.

[32] For each site, temperature and relative humidity values are available at a number of pressure levels for the model and radiosonde data. These data were first interpolated to a regular 50 hPa pressure grid. Above the uppermost level, temperature and water vapor mass mixing ratios were prescribed from a mean tropical profile [McClatchey *et al.*, 1972], with a vertical resolution of 1 km. At other levels, water vapor mass mixing ratios were calculated from the temperature and relative humidity data. The

model temperature and relative humidity profiles and the mean and root mean squared (RMS) differences between radiosonde and model profiles are presented for Brindisi (Figure 6) and for St. Helena (Figure 7) for June 2004 1200 UTC data. The profiles at Brindisi are generally moist throughout with temperature and moisture errors generally larger in the upper troposphere. The profiles at St. Helena are extremely dry above a moist boundary layer.

[33] Calculations were subsequently performed using the model and radiosonde profiles as input to the version

Table 2. Calculated Clear-Sky OLR and Clear-Sky Albedo at the Top of the Atmosphere for Model Profiles and Flux Differences Calculated by Applying Observed Minus Model Profile Differences and RMS Differences and Changes in Aerosol and Surface Albedo for Selected Radiosonde Sites

Site	Longitude	Latitude	OLR_m , ^a W m ⁻²	ΔOLR , ^b W m ⁻²	ΔOLR_T , ^c W m ⁻²	ΔOLR_q , ^d W m ⁻²	ΔOLR_{aer} , ^e W m ⁻²	ISW, ^f W m ⁻²	α_m , ^a %	$\Delta\alpha_q$, ^d %	$\Delta\alpha_{aer}$, ^e %	$\Delta\alpha_{cs}$, ^f %
Santa Rita	27.1°W	38.7°N	268.9	2.0	2.3	-4.9	0.8	1189	6.81	-0.02	-0.37	0.33
Funchal	16.9°W	32.6°N	283.3	1.6	2.5	-6.0	0.9	1272	6.35	-0.03	-0.10	0.34
Sal	23.0°W	16.7°N	290.7	5.9	2.3	-8.0	0.8	1237	6.55	-0.05	-0.21	0.34
Brindisi	18.0°E	40.3°N	273.4	0.4	2.3	-4.8	0.8	1202	6.72	-0.02	-0.32	0.33
St. Helena	5.1°W	15.9°S	296.3	2.6	3.3	-9.1	0.9	1032	7.85	-0.03	-0.96	0.33
Ascension	14.4°W	8.0°S	293.3	-3.3	2.9	-6.3	0.9	1110	7.23	-0.03	-0.63	0.33

^a OLR_m and α_m are the clear-sky OLR and albedo calculated using model profiles.

^b ΔOLR and $\Delta\alpha$ are the radiosonde profile minus model profile clear-sky OLR and albedo differences.

^c ΔOLR_T is the calculated OLR difference when the model RMS temperature errors are added to the model temperature profiles.

^d ΔOLR_q and $\Delta\alpha_q$ are the calculated OLR or α differences when model RMS moisture errors are added to the model profiles.

^e ΔOLR_{aer} and $\Delta\alpha_{aer}$ are the OLR and albedo differences on removing climatological aerosols from the model atmosphere.

^f $\Delta\alpha_{cs}$ is the change in clear-sky albedo on increasing surface albedo by 0.005 (0.5%).

of the *Edwards and Slingo* [1996] radiation code used in the NWP model. Nine bands were applied in the longwave spectrum and six bands in the shortwave spectrum. Ozone concentrations were interpolated from the *McClatchey et al.* [1972] tropical profile. Remaining trace gases were prescribed at current day concentrations and climatological aerosol concentrations were applied, consistent with the forecast model. The surface emissivity was set to unity and a surface albedo of 0.04 (4%) was assumed.

[34] A number of sensitivity studies were performed to investigate the likely error in the model clear-sky fluxes. First, clear-sky OLR and albedo at the top of the atmosphere were calculated for the model profiles and the radiosonde profiles. The model profiles were then perturbed by the RMS temperature error and also the water vapor mass mixing ratio calculated from the RMS relative

humidity errors. The RMS errors provide information on the likely instantaneous errors in model temperature and humidity. However, while instantaneous errors may be of different sign throughout the profiles, the RMS errors instead assume a consistent sign throughout the profile, so providing an estimate of the maximum likely error in terms of the radiative flux perturbation. Calculations of the clear-sky OLR and albedo were performed separately for each case.

[35] Additionally, the sensitivity of the OLR and albedo to the removal of the climatological aerosol profiles was computed using the model profiles. Finally, the sensitivity of the clear-sky albedo to an increase in surface albedo of 0.005 was calculated. The ocean surface albedo and its likely error for low-latitude regions is approximated using the results of *Jin et al.* [2002]. The results of the radiative computations are summarized in Table 2.

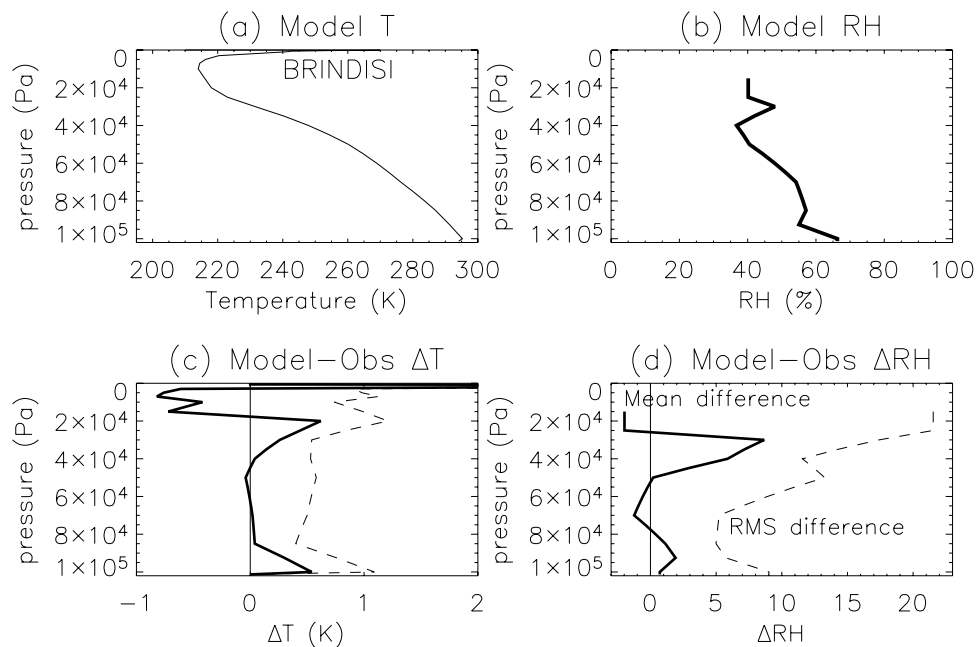


Figure 6. Model vertical profiles of (a) temperature and (b) relative humidity and the model minus observation difference and RMS difference in (c) temperature and (d) relative humidity for Brindisi (18°E, 40.3°N), June 2004.

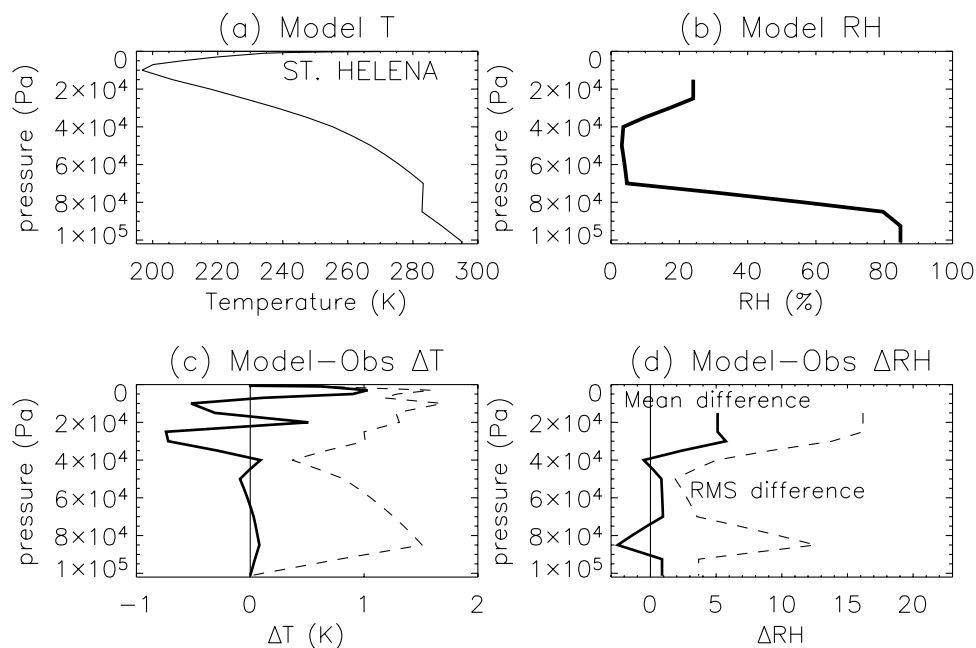


Figure 7. As in Figure 6 but for St. Helena (5.1°W, 15.9°S).

[36] The mean OLR differences calculated from the radiosonde minus model profiles range from -3.3 W m^{-2} to 5.9 W m^{-2} . The sensitivity of clear-sky albedo to the radiosonde minus model profiles is less than 0.01% (not shown). Perturbing the model temperature profiles by the RMS error gives rise to an OLR difference of about 3 W m^{-2} . Perturbing the moisture profile using the RMS humidity errors leads to a larger OLR sensitivity between 4.8 and 9.1 W m^{-2} and a small albedo sensitivity of 0.05% or less. The sensitivity of model OLR to the removal of climatological aerosol is less than 1 W m^{-2} while the change in clear-sky albedo to the removal of climatological aerosol ranges from -0.1% to -0.96% with the larger sensitivity corresponding with the lower ISW (highest solar zenith angle).

[37] We conclude from the results presented in Table 2 that a probable error in clear-sky OLR of order $\pm 5\text{--}10 \text{ W m}^{-2}$ (approximately 3.5% of tropical ocean mean clear-sky OLR) and a probable error in clear-sky albedo of order $\pm 1\%$ (approximately 15% of tropical mean clear-sky albedo) are reasonable estimates.

5.2. Time Series

[38] Keeping in mind the above estimates of expected model error in clear-sky OLR and albedo, we now compare clear-sky collocated radiative fluxes from GERB and the model. Time series of 1200 UTC GERB and model clear-sky OLR and albedo and the differences are examined for two distinct regions: the south Atlantic (30–0°W, 10–30°S) and the Mediterranean (0–40°E, 30–45°N). To reduce errors relating to poor geolocation we use ARG data and only consider ocean grid points that are not adjacent to land points.

[39] Figure 8a shows clear-sky OLR from GERB (Δ) and the model (+) averaged from all the grid points within the region in which both model and SEVIRI cloud fraction

are zero. The solid line denotes the area average of the model diagnostic clear-sky OLR, which is calculated for all oceanic grid points within the region regardless of cloud fraction. The difference between the solid line and the crosses therefore represents the effect of clear-sky sampling on the model output [e.g., *Allan and Ringer, 2003*]. For example, if the clear pixels within the entire region are systematically warmer or drier than the mean for the whole region, the clear-sky sampled model clear-sky OLR (+) will be higher than the model diagnostic clear-sky OLR (solid line). Thus it is clear from Figure 8a that the spatial sampling of grid points is important in determining clear-sky OLR. This reinforces the need to sample consistently when comparing model and satellite data in this manner, particularly in this case where coincident cloud-free model and observational pixels often cover only a fraction of the region considered. Figure 8b shows a similar comparison for clear-sky albedo. The slowly varying model diagnostic clear-sky albedo is primarily due to the solar zenith angle dependence of surface albedo. The changes in diagnostic clear-sky OLR in Figure 8a relate to changes in area mean relative humidity and, especially for longer term variations, changes in sea surface temperature (SST).

[40] Figures 8c and 8d show time series of GERB minus model clear-sky OLR and albedo differences. For June and July 2003 there are sometimes large positive differences. For example, an arrow in Figures 8b and 8d denotes a high GERB albedo value of 0.2 and GERB minus model albedo difference of 0.11. These differences coincide with version 1 MS7A data (Table 1), which were prone to large geolocation errors. The higher GERB albedo is therefore very likely to be explained by a cloudy GERB pixel being misregistered with a clear-sky Meteosat-7 imager pixel. However, for much of the time series, clear-sky albedo differences are generally small, although GERB systemat-

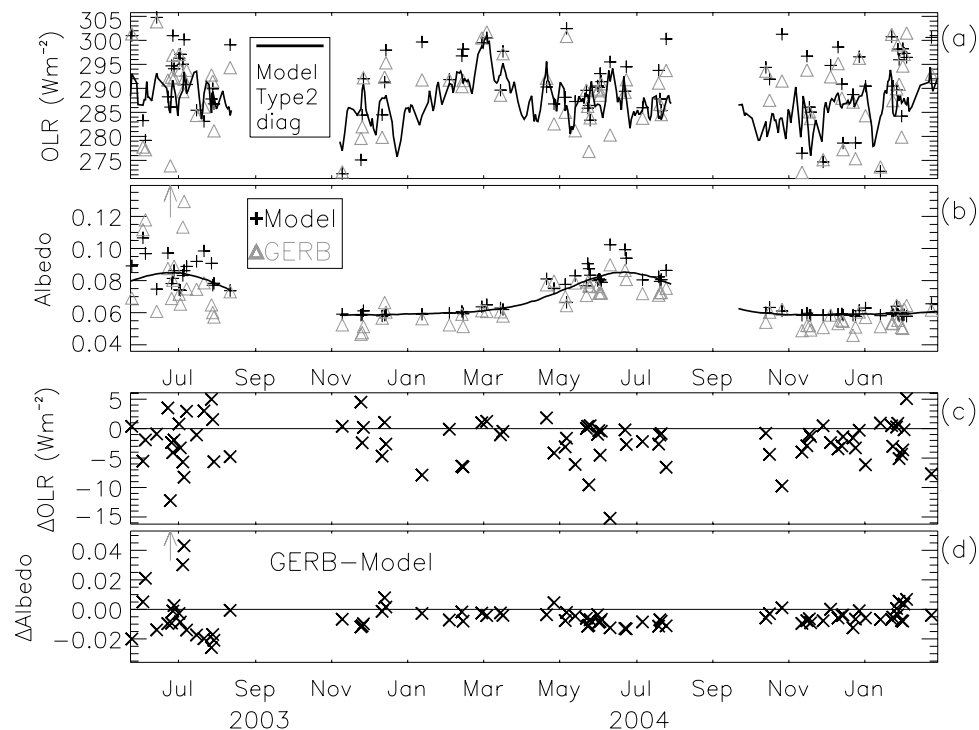


Figure 8. GERB and model clear-sky (a) OLR and (b) Albedo and GERB minus model clear-sky (c) OLR and (d) albedo differences for the South Atlantic ($10\text{--}30^\circ\text{W}$, $10\text{--}30^\circ\text{S}$) using ARG data. See color version of this figure in the HTML.

ically estimates albedo values approximately 0.01 (or 1%) less than the model values. This is of the same magnitude of the expected model error in clear-sky albedo approximated from Table 2 based on the prescribed changes in aerosol and surface albedo. Clear-sky OLR differences are generally less than 5 W m^{-2} , which is smaller than the expected clear-sky OLR model error. This suggests that GERB clear-sky OLR fluxes over the open ocean are unlikely to be erroneous.

[41] We now repeat the time series analysis on the Mediterranean region. Figure 9a shows a large change in clear-sky OLR over the season in both model estimates and the GERB measurements. This relates to the larger changes in SST experienced over the Mediterranean compared with the South Atlantic. There is also an abundance of clear-sky situations, especially during summer, for the Mediterranean region.

[42] Consistent with the south Atlantic comparison, the June 2003 data show large positive GERB minus model differences in clear-sky albedo, which are most likely due to cloud contamination. Additionally, the poor geolocation may also have caused bright land surfaces to be misregistered as open ocean regions, which will also cause GERB to appear to overestimate albedo compared to the model clear-sky values. However, unlike the south Atlantic comparison, throughout the time series there are events in which differences are larger than expected model errors in clear-sky OLR of $\pm 5\text{--}10\text{ W m}^{-2}$ and clear-sky albedo (± 0.01). Since April 2004, smaller model-observed differences of $\pm 5\text{ W m}^{-2}$ in clear-sky OLR and ± 0.01 in clear-sky albedo are apparent, suggesting that any bias in GERB

clear-sky albedo is within the model error. A larger GERB minus model clear-sky OLR difference of about 10 W m^{-2} is evident from late January 2005; it is possible that this may relate to changes in the model implemented on 18 January 2005 (see Table 1).

[43] The Meteosat-7 and SEVIRI-based cloud masks used are based upon visible channels only available during daylight hours. Therefore comparisons of clear-sky fluxes at night were not possible. However, we did examine the clear-sky ocean fluxes over the Mediterranean at 0600 UTC and for the south Atlantic at 1800 UTC which contain local daytime data (not shown). The OLR variations and differences are found to be very similar to the 1200 UTC comparisons described above. The magnitude of albedo and albedo differences for 0600 UTC and 1800 UTC comparisons are larger than for 1200 UTC because of the higher solar zenith angles. However, the seasonal variations and sign of the clear-sky albedo differences otherwise appear consistent between the different analysis times.

[44] Finally, it is important to note that the temporal evolution of clear-sky flux differences in Figures 8 and 9 show no evidence for significant long-term drift in the calibration of the GERB instrument.

5.3. Spatial Scatter

[45] Figure 10 shows the scatterplot of clear-sky OLR and clear-sky albedo over the ocean for collocated GERB ARG and model 1200 UTC data during June 2004. Again, we only consider grid points where both model and SEVIRI cloud fraction are zero over open ocean regions. There is

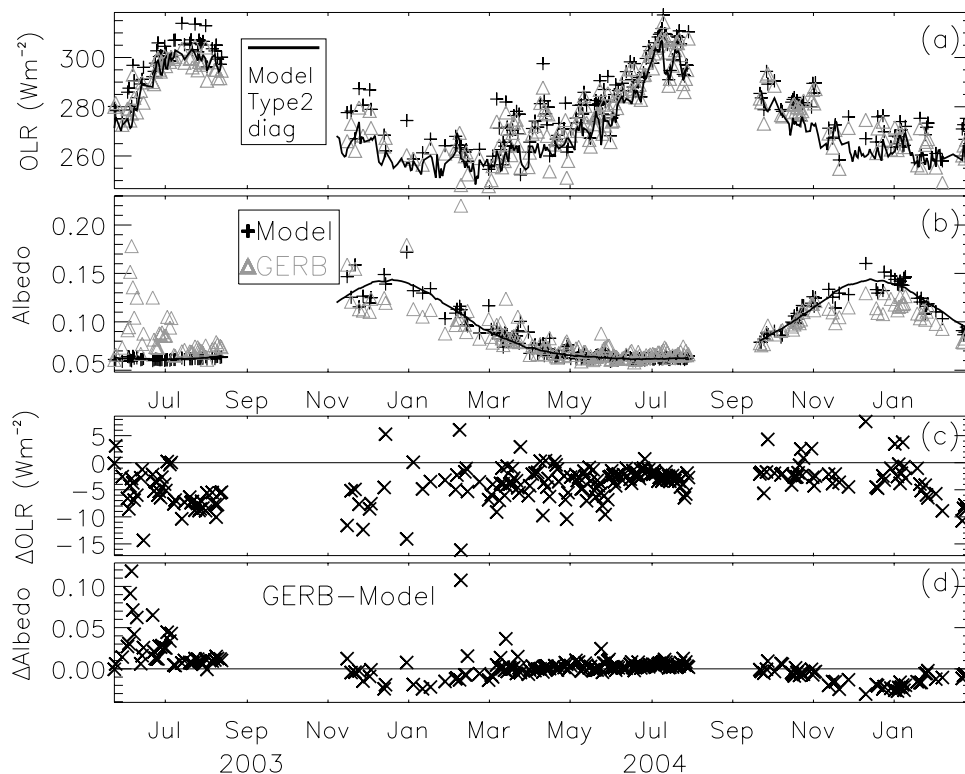


Figure 9. As in Figure 8 but for the Mediterranean ($0\text{--}40^{\circ}\text{E}$, $30\text{--}45^{\circ}\text{N}$). See color version of this figure in the HTML.

excellent agreement between model and GERB clear-sky OLR (Figure 10a) with an RMS error of 3.5 W m^{-2} (around 1% of tropical ocean clear-sky OLR), well within the expected model error in clear-sky OLR. Differences for January 2004 and for 0600 UTC and 1800 UTC comparisons for June 2004 give a larger RMS difference of about 5 W m^{-2} (not shown). However all months and analysis times for 2004 show a similar scatter distribution with a tendency for positive model minus GERB differences. This is consistent with the regional comparisons presented in the previous section.

[46] Also plotted in Figure 10a are the clear-sky OLR values calculated from the model and radiosonde profiles (x axis) presented in Table 2. Error bars for the model fluxes at each station are constructed by calculating the RMS of the error estimates, ΔOLR_T , ΔOLR_q , and ΔOLR_{aer} described in Table 2. From the results presented in Figure 10a we conclude that the clear-sky OLR given by GERB is within the model uncertainty based on the analysis of observed minus analysis temperature and moisture profile errors.

[47] Differences in clear-sky albedo (Figure 10b) show more scatter than the clear-sky OLR comparison, with both June and January (not shown) 2004 exhibiting a RMS difference of about 0.01 (or about 10% of tropical clear-sky albedo). A larger RMS difference of 0.02 occurs for 0600 UTC and 1800 UTC data for June 2004 with positive model minus GERB clear-sky albedo differences dominating for 1800 UTC data (not shown).

[48] For the June 2004 1200 UTC comparison, there are many situations for model clear-sky albedo of $0.06\text{--}0.07$

where GERB estimates of clear-sky albedo are larger by 0.02. This may relate to cloud contamination of the GERB data or gross underestimates in the aerosol optical depth prescribed in the model. On the basis of the results of *Jin et al.* [2002] and the calculations made in Table 2 it is unlikely that errors in the model surface albedo can explain this discrepancy. It therefore remains a possibility that errors exist in the GERB data for low solar zenith angles (note that clear-sky albedo over the ocean increases with solar zenith angle).

[49] At higher solar zenith angles (e.g., lower solar elevation), model clear-sky albedo tends to be systematically larger than the GERB data by as much as 0.03. This cannot be explained by cloud contamination and is unlikely to be related to surface albedo errors. These positive differences primarily originate from the southern hemisphere further south than 10°S . The time series of clear-sky albedo differences over the south Atlantic (Figure 8) also tends to display a negative GERB minus model clear-sky albedo difference of around -0.01 during June 2004. Higher solar zenith angles are associated with larger potential errors in surface albedo [e.g., *Jin et al.*, 2002] and larger clear-sky albedo difference in response to an aerosol profile error. The change in aerosol-related albedo error with ISW is reflected in Table 2 and also by the estimated albedo error, denoted by error bars and calculated as the RMS of $\Delta\alpha_{aer}$ and $\Delta\alpha_{cs}$ from Table 2, in Figure 10b for Funchal, Brindisi, and St. Helena. Because the SEVIRI cloud fraction developed by *Ipe et al.* [2004] may class high aerosol optical depth events as cloud over ocean regions (N. Bellouin, personal communication, 2004), the positive model minus

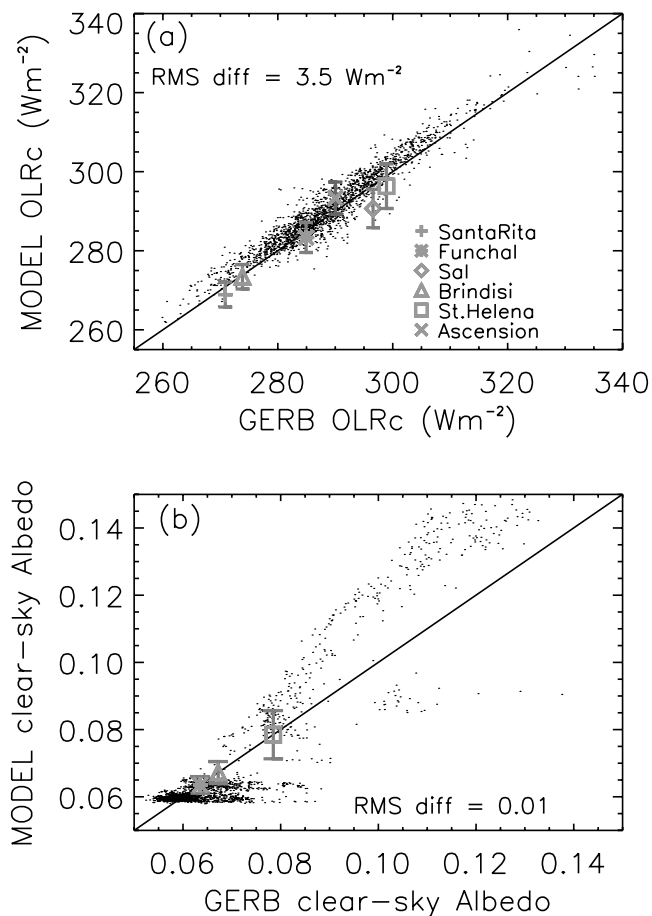


Figure 10. GERB (ARG) and model (a) OLRc and (b) Clear-sky albedo over the open ocean for June 2004 1200 UTC data. Also plotted are calculations using model and observed profiles at particular sites with estimates of model error. See color version of this figure in the HTML.

GERB clear-sky albedo for higher solar zenith angles may be explained by the systematic sampling of pristine conditions by the clear-sky sampling method used compared to climatological average aerosol used in the model. However, further analysis is required to confirm the reasons for these albedo differences.

6. Conclusions

[50] A methodology is described that facilitates comparisons in near-real time (within one day) of broadband radiative fluxes from the Geostationary Earth Radiation Budget (GERB) instrument and simulated from the Met Office forecast model analyses.

[51] Initial results highlight a variety of differences between the model simulations of top of atmosphere shortwave albedo and outgoing longwave radiation, relating to possible errors in model cloud fields in the tropics and subtropics and surface fields over north Africa. However, because the GERB data are currently under validation, the details of these differences are not discussed at length and will be presented more extensively in future

papers. Instead in the present study we concentrate on using the model simulations of clear-sky radiative fluxes over the ocean, combined with additional data from radiosonde soundings used in the assimilation process, to assess the quality of the GERB clear-sky fluxes over the ocean.

[52] We use model and radiosonde vertical profiles of temperature and humidity to provide input to the *Edwards and Slingo* [1996] radiation code and undertake a variety of sensitivity tests to assess the expected error in model clear-sky OLR and clear-sky albedo over the ocean. Estimates of clear-sky OLR errors are of order ± 5 – 10 W m^{-2} , while probable errors in clear-sky top of atmosphere albedo are of magnitude ± 0.01 .

[53] Analyzing time series of clear-sky OLR and albedo at 1200 UTC over the south Atlantic and the Mediterranean, a general reduction in GERB minus model differences was found, relating to the improving quality of the GERB data after initial problems with geolocation accuracy and inferior radiance to flux processing. Data after April 2004 appear to produce the lowest differences in clear-sky fluxes, with clear-sky albedo differences smaller than 0.02 and clear-sky OLR differences less than about 5 W m^{-2} . Analyzing data for June 2004 at 1200 UTC, a RMS clear-sky OLR difference of 3.5 W m^{-2} is well within the expected model errors due to temperature, moisture and aerosol uncertainty. A clear-sky albedo RMS difference of 0.01 is of similar magnitude to the expected model error relating to expected aerosol and surface albedo errors.

[54] On the basis of the comparison of clear-sky fluxes between the model and GERB data we find no reason to believe that the recent clear-sky OLR data derived from GERB are erroneous. While clear-sky albedo differences are larger, the differences are of similar magnitude to the expected model errors over most regions. On the basis of the analyses of the time series of clear-sky OLR and albedo differences, there is also no evidence for significant long-term drift in the calibration of the instrument. GERB minus model albedo differences for clear-sky ocean regions are generally positive for the Mediterranean and negative for the South Atlantic regions. There is also a tendency for positive model minus GERB clear-sky albedo differences to dominate for 1800 UTC comparisons. Ongoing analysis indicates asymmetries in the GERB derived albedo that may relate to errors in the angular dependence model used to estimate fluxes from radiances (J. Futyán, personal communication, 2004). Further analysis of clear-sky shortwave albedo over the ocean is required to identify diurnal errors in the GERB data.

[55] While initial comparisons of model, GERB and CERES fluxes for all-sky conditions suggest that the GERB data are reasonable, the validation of the cloudy-sky fluxes are beyond the scope of the present study and will be assessed elsewhere. Once the quality of GERB radiative fluxes has been ascertained, future studies will begin to exploit these data along with complementary imager data from the SEVIRI instrument to evaluate the simulation of clouds, water vapor and surface properties in the model. It is also planned to include simulations of selected channels from SEVIRI using the radiance code described by *Ringer et al.* [2002], to analyze forecasts from the Met Office NWP

model and to utilize measurements of radiative fluxes at the surface.

[56] **Acknowledgments.** This work was funded through the NERC/Met Office Connect-B grant NER/D/S/2002/00412. Thanks are owed to Jacqui Russell, Joanna Futyran, John Harries, Nicolas Clerbaux, Steve Dewitte, and the GERB International Science Team and to Mark Ringer, Jim Haywood, Damian Wilson, John Edwards, and Malcolm Brooks at the Met Office for valuable discussions and input. The CERES data were retrieved from the NASA Langley DAAC. The GERB data were retrieved from the Royal Meteorological Institute of Belgium, who also provided valuable advice. We thank two anonymous reviewers for their comments.

References

- Allan, R. P., and M. A. Ringer (2003), Inconsistencies between satellite estimates of longwave cloud forcing and dynamical fields from reanalyses, *Geophys. Res. Lett.*, *30*(9), 1491, doi:10.1029/2003GL017019.
- Allan, R. P., M. A. Ringer, J. A. Pamment, and A. Slingo (2004a), Simulation of the Earth's radiation budget by the European Centre for Medium-Range Weather Forecasts 40-year reanalysis (ERA40), *J. Geophys. Res.*, *109*, D18107, doi:10.1029/2004JD004816.
- Allan, R. P., A. Slingo, S. Milton, I. Culverwell (2004b), SINERGEE, simulation and exploitation of data from Meteosat-8 using an NWP model, paper presented at the 2004 EUMETSAT Meteorological Satellite Conference, Eur. Organ. for the Exploit. of Meteorol. Satell., Prague, Czech Republic.
- Bell, R. S., S. Milton, C. Wilson, and T. Davies (2002), A new unified model, in *NWP Gazette*, pp. 3–7, Met Off., Reading, U. K., June. (Available at http://www.metoffice.gov.uk/research/nwp/publications/nwp_gazette/jun02/index.html)
- Bushell, A. C., and G. M. Martin (1999), The impact of vertical resolution upon GCM simulations of marine stratocumulus, *Clim. Dyn.*, *15*, 293–318.
- Edwards, J. M., and A. Slingo (1996), Studies with a flexible new radiation code. I: Choosing a configuration for a large-scale model, *Q. J. R. Meteorol. Soc.*, *122*, 689–719.
- Essery, R. L. H., M. J. Best, R. A. Betts, P. M. Cox, and C. M. Taylor (2003), Explicit representation of subgrid heterogeneity in a GCM land surface scheme, *J. Hydrometeorol.*, *4*, 530–543.
- Fritsch, J. M., and C. F. Chappell (1980), Numerical prediction of convectively driven mesoscale pressure systems. part I: Convective parametrization, *J. Atmos. Sci.*, *37*, 1722–1733.
- Grant, A. L. M. (2001), Cloud base mass fluxes in the cumulus capped boundary layer, *Q. J. R. Meteorol. Soc.*, *127*, 407–421.
- Grant, A. L. M., and A. R. Brown (1999), A similarity hypothesis for cumulus transports, *Q. J. R. Meteorol. Soc.*, *125*, 1913–1935.
- Harries, J. E., et al. (2005), The Geostationary Earth Radiation Budget Project (GERB), *Bull. Am. Meteorol. Soc.*, *86*, 945–960.
- Haywood, J. M., R. P. Allan, I. Culverwell, A. Slingo, S. F. Milton, J. M. Edwards, and N. Clerbaux (2005), Can desert dust explain the outgoing longwave radiation anomaly over the Sahara during July 2003?, *J. Geophys. Res.*, *110*, D05105, doi:10.1029/2004JD005232.
- Intergovernmental Panel on Climate Change (2001), *Climate Change 2001: The Scientific Basis*, edited by J. T. Houghton et al., Cambridge Univ. Press, New York.
- Ipe, A., N. Clerbaux, C. Bertrand, S. Dewitte, and L. Gonzalez (2004), Validation and homogenisation of cloud optical depth and cloud fraction retrievals for GERB/SEVIRI scene identification using Meteosat-7 data, *Atmos. Res.*, *72*, 17–37, doi:10.1016/j.atmosres.2004.03.010.
- Jin, Z., T. P. Charlock, and K. Rutledge (2002), Analysis of broadband solar radiation and albedo over the ocean surface at COVE, *J. Atmos. Oceanic Technol.*, *19*, 1585–1596.
- Kiehl, J. T., and D. L. Williamson (1991), Dependence of cloud amount on horizontal resolution in the NCAR Community Climate Model, *J. Geophys. Res.*, *96*, 10,955–10,980.
- Kiehl, J. T., J. J. Hack, and B. P. Briegleb (1994), The simulated Earth radiation budget of the National Center for Atmospheric Research Community Climate Model CCM2 and comparisons with the Earth Radiation Budget Experiment (ERBE), *J. Geophys. Res.*, *99*, 20,815–20,827.
- Lane, D. E., R. C. Somerville, and S. F. Iacobellis (2000), Sensitivity of cloud and radiation parametrizations to changes in vertical resolution, *J. Clim.*, *13*, 915–922.
- Lock, A. P., A. R. Brown, M. R. Bush, G. M. Martin, and R. N. B. Smith (2000), A new boundary layer mixing scheme. part I: Scheme description and single-column model tests, *Mon. Weather Rev.*, *128*, 3187–3199.
- Lorenc, A. C., et al. (2000), The Met Office global three-dimensional variational data assimilation scheme, *Q. J. R. Meteorol. Soc.*, *126*, 2991–3012.
- Martin, G. M., M. R. Bush, A. R. Brown, A. P. Lock, and R. N. B. Smith (2000), A new boundary layer mixing scheme. part II: Tests in climate and mesoscale models, *Mon. Weather Rev.*, *128*, 3200–3217.
- McClatchey, R. A., R. A. Fenn, R. A. Selby, P. E. Voltz, and J. S. Garing (1972), Optical properties of the atmosphere, *Environ. Res. Pap.* *411*, 107 pp., Air Force Cambridge Res. Lab., Bedford, Mass.
- Milton, S. F., and C. A. Wilson (1996), The impact of parametrized subgridscale orographic forcing on systematic errors in a global NWP model, *Mon. Weather Rev.*, *124*, 2023–2045.
- Morcrette, J.-J. (1991), Evaluation of model-generated cloudiness: Satellite observed and model-generated diurnal variability of brightness temperature, *Mon. Weather Rev.*, *119*, 1205–1224.
- Phillips, T. J., L. C. Corsetti, and S. L. Grotch (1995), The impact of horizontal resolution on moist processes in the ECMWF model, *Clim. Dyn.*, *11*, 85–102.
- Pope, V. D., and R. Stratton (2002), The processes governing horizontal resolution sensitivity in a climate model, *Clim. Dyn.*, *19*, 211–236.
- Pope, V. D., M. L. Gallani, P. R. Rowntree, and R. A. Stratton (2000), The impact of new physical parametrizations in the Hadley Centre climate model: HadAM3, *Clim. Dyn.*, *16*, 123–146.
- Ringer, M. A., J. M. Edwards, and A. Slingo (2002), Simulations of satellite channel radiances in the Met Office Unified Model, *Q. J. R. Meteorol. Soc.*, *129*, 1169–1190.
- Schmetz, J., P. Pili, S. Tjemkes, D. Just, J. Kerkmann, S. Rota, and A. Ratier (2002), An introduction to Meteosat second generation (MSG), *Bull. Am. Meteorol. Soc.*, *83*, 977–992.
- Slingo, A., K. I. Hodges, and G. R. Robinson (2004), Simulation of the diurnal cycle in a climate model and its evaluation using data from Meteosat 7, *Q. J. R. Meteorol. Soc.*, *130*, 1449–1467.
- Soden, B. J., R. T. Wetherald, G. L. Stenchikov, and A. Robock (2002), Global cooling after the eruption of Mount Pinatubo: A test of climate feedback by water vapor, *Science*, *296*, 727–730.
- Webb, M., C. Senior, S. Bony, and J.-J. Morcrette (2001), Combining ERBE and ISCCP data to assess clouds in the Hadley Centre, ECMWF and LMD atmospheric climate models, *Clim. Dyn.*, *17*, 905–922.
- Webster, S., A. R. Brown, D. R. Cameron, and C. P. Jones (2003), Improvements to the representation of orography in the Met Office Unified Model, *Q. J. R. Meteorol. Soc.*, *129*, 1989–2010.
- Wilson, D. R., and S. P. Ballard (1999), A microphysically based precipitation scheme for the U.K. Meteorological Office Unified Model, *Q. J. R. Meteorol. Soc.*, *125*, 1607–1636.
- Wielicki, B. A., B. R. Barkstrom, E. F. Harrison, R. B. Lee, G. L. Smith, and J. E. Cooper (1996), Clouds and the Earth's Radiant Energy System (CERES): An Earth Observing System experiment, *Bull. Am. Meteorol. Soc.*, *77*, 853–868.
- Yang, G.-Y., and J. Slingo (2001), The diurnal cycle in the tropics, *Mon. Weather Rev.*, *129*, 784–801.

R. P. Allan and A. Slingo, Environmental Systems Science Centre, University of Reading, Harry Pitt Building, Whiteknights, PO Box 238, Reading, RG6 6AL, UK. (rpa@mail.nerc-essc.ac.uk)

I. Culverwell and S. F. Milton, Met Office, FitzRoy Road, Exeter, EX1 3PB, UK.